Article

Probabilistic Seismic Assessment of CoSPSW Structures Using Fragility Functions

Zhilun Tan [1], Qiuhong Zhao [1,2,*] , Yu Zhao [3] and Cheng Yu [4]

1   School of Civil Engineering, Tianjin University, Tianjin 300350, China; zltan@tju.edu.cn
2   Key Laboratory of Coast Civil Structure and Safety of Ministry of Education, Tianjin University, Tianjin 300350, China
3   China Railway Design Corporation Co., Ltd., Tianjin 300308, China; yuzhao@tju.edu.cn
4   Department of Mechanical Engineering, University of North Texas, Denton, TX 76207, USA; cheng.yu@unt.edu
*   Correspondence: qzhao@tju.edu.cn

Abstract: The corrugated steel plate shear wall (CoSPSW) is a new type of steel plate shear wall, in which corrugated wall plates instead of flat wall plates are adopted. The lateral stiffness and shear buckling capacity of the shear wall system could be significantly enhanced, and then, wall plate buckling under gravity loads would be mitigated. This paper presents a study on the probabilistic assessment of the seismic performance and vulnerability of CoSPSWs using fragility functions. The damage states and corresponding repair states of CoSPSWs were first established from experimental data. Then, incremental dynamic analyses were conducted on the CoSPSW structures. The structural and nonstructural fragility functions were developed, based on which the seismic performance and vulnerability of the CoSPSWs were obtained and compared with the conventional steel plate shear walls (SPSWs). It was shown that for various repair states, the 25th percentile PGA of the CoSPSW was always higher than the SPSWs with the same wall thickness and boundary frame, which indicated that the CoSPSW has a lower damage potential and better seismic performance than the SPSW.

Keywords: corrugated steel plate shear wall; damage state; repair state; fragility function; probabilistic assessment

1. Introduction

Steel plate shear walls (SPSWs) were proposed in the 1970s as new lateral load-resisting systems for mid- to high-rise buildings, with advantages such as high lateral strength, ductility, and energy dissipation capacity [1–3]. Originally, the SPSW was composed of flat infill wall plates, boundary beams, and boundary columns, while the wall plates were generally slender and tended to buckle under low lateral loads or gravity loads in a serviceability limit state, which was related to wall out-of-plane deformation and an unpleasant buckling noise. The ultimate lateral strength of the wall plate would then be achieved through the yielding of the diagonal tension field formed due to wall buckling under lateral loads [4], which also resulted in high anchoring forces on the boundary frame [5]. On the other hand, wall buckling under gravity loads or during construction is not permitted by the Chinese code [6], which prohibits a synchronized installation of the wall plate with the rest of the story, and this hinders the construction schedule, especially for high-rise buildings.

Corrugated steel plate shear walls (CoSPSWs) could be a viable solution in that sense; they consist of horizontally or vertically corrugated wall plates and a boundary frame [7], as shown in Figure 1. The corrugation significantly increases the out-of-plane stiffness and buckling strength of the wall plate, which would then resist the lateral loads through in-plane shear instead of tension field action. In addition, due to the "accordion effects", axial

stiffness will be at its minimum when perpendicular to the rib and greatly enhanced when parallel to the rib. In addition, horizontal or vertical corrugation could either minimize or resist the vertical stresses transferred to the wall plates from gravity loads and thus avoid buckling during construction. Therefore, corrugated wall plates could be erected simultaneously with the rest of the story and considerably increase construction speed, especially for high-rises.
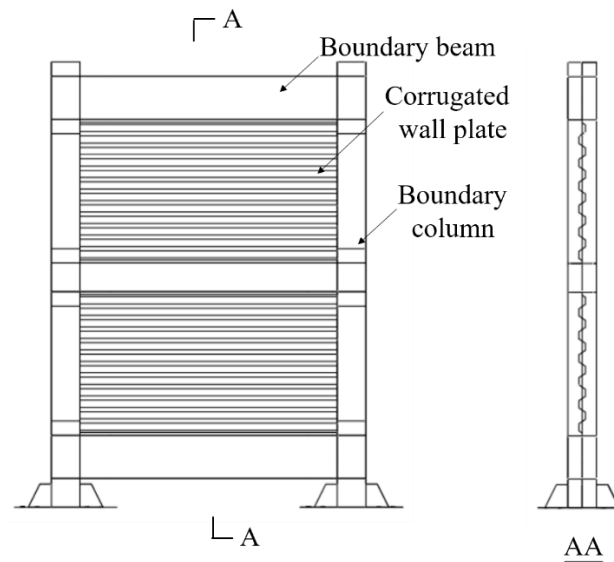

Figure 1. Corrugated steel plate shear wall.

Experimental [8–17] and numerical analysis [18–23] have been conducted on the cyclic and lateral behavior of CoSPSWs and have revealed that the hysteresis curve pinching of flat wall plates could be obviously improved and energy dissipation could be increased accordingly [20,21], and the corrugated wall plates could even achieve shear yielding sometimes, which significantly lowered the anchoring forces on the boundary frame [15]. Furthermore, extended research has been conducted on corrugated steel shear walls with perforations or openings [24–27], a reduced beam section [28,29], a semi-rigid boundary frame [30], and a low-yield-point steel wall panel [31], as well as on the application of corrugated steel shear walls in a modular structural design [32]. A performance-based seismic design (PBSD) procedure has also been proposed [33], and time-history analyses have revealed that the inter-story drift of the CoSPSW with PBSD distributed more smoothly than the CoSPSW with a traditional design, which helped to avoid weak stories.

In order to acquire a rational estimation of potential seismic losses, the seismic performance of structures could be quantitatively evaluated through a probabilistic assessment method, which is realized by developing analytical fragility functions. Fragility functions are statistical models that could predict the possibility of structures reaching or exceeding different damage states under different earthquake intensities; therefore, they could characterize the seismic performance of structures quantitatively and describe the relationship between the earthquake intensity and the damage state of structures.

Researchers have conducted probabilistic seismic assessment on various wall structures and evaluated their seismic performance by developing fragility functions for different damage states or repair states. Baldvins et al. [34] established twelve damage states and five repair states of SPSWs based on experimental results and observations and developed the fragility functions for each repair state. Negar et al. [35] established five damage states and the corresponding repair states of steel-plate concrete composite shear walls based on experimental results and observations and derived the fragility functions for the damage states associated with concrete crushing and faceplate fracture. Wang et al. [36] conducted incremental dynamic analyses on coupled low-yield-point steel plate shear walls, based

on which six damage states were established and fragility functions were developed for different damage states.

In addition, probabilistic seismic assessment was conducted on structural frames retrofitted with different types of steel walls or panels using fragility functions for different damage states or repair states. Zhang et al. [37] conducted time-history analyses on retrofitted SPSW systems in order to develop the fragility functions and found that the SPSW with low-yield-point steel wall plates had lower seismic vulnerability than the SPSW with ordinary steel wall plates. Jiang et al. [38,39] conducted incremental dynamic analyses on steel frames retrofitted with steel panels and developed the fragility functions and validated the effectiveness of adding steel panels to reduce the seismic vulnerability of existing steel frame buildings. Bu et al. [40] conducted incremental dynamic analyses on steel frames equipped with four different types of steel slit shear walls and developed the fragility functions, and the type with best performance was identified for all damage states. Currently, research on the probabilistic seismic assessment of CoSPSWs is still very limited.

In this paper, the seismic performance of CoSPSWs will be quantitatively evaluated through the probabilistic assessment method using fragility functions, which has not been reported in current literature. The damage states and corresponding repair states of CoSPSWs will first be established through experimental results and test observations. Then, incremental dynamic analyses will be conducted on a 10-story CoSPSW using PBSD, based on which analytical fragility functions will be developed for the different damage and repair states of structural and nonstructural components. Finally, the seismic performance and vulnerability of the CoSPSW and the SPSW are evaluated and compared probabilistically using the fragility functions.

2. Damage States and Repair States

2.1. Establishment of Damage States and Repair States

The seismic performance and the vulnerability of the structures can be assessed through the probabilistic assessment, which estimates the probabilistic structural response, i.e., the engineering demand parameter (EDP) as a function of ground motion intensity, i.e., the intensity measure (IM), and uses quantitative measures to evaluate the structural and nonstructural performance under seismic loads [37]. Therefore, first it is necessary to determine the engineering demand parameter, which could be peak inter-story drift, peak floor acceleration or ductility, etc. As the peak inter-story drift and the peak floor acceleration are used for seismic loss estimation in HAZUS-MH MR5 [41], these two structural response factors were chosen as the engineering demand parameter (EDP) in this study. The geometry and peak inter-story drift of 19 corrugated steel plate shear wall specimens from nine cyclic tests are summarized and shown in Table 1 below.

From the test observations on the 19 specimens listed in Table 1 and the relevant damage states of SPSW [34], 12 damage states (DS1–DS12) and 5 repair states (RS1–RS5) were established to describe the damage degree of the CoSPSW specimens and determine the corresponding repair methods, as shown in Tables 2 and 3. For damage states DS1,2,4,5, and 6, structural repair is not necessary as there is no permanent residual deformation. For damage states DS 3 and 9, the corrugated web plate suffers relatively severe damage and cannot recover the initial state. Thus, the infilled corrugated web plate needs to be replaced. For DS7,8,10, and 11, FEMA 352 (FEMA 2000) [42] recommends that the frame members should be repaired when the buckling degree exceeds tolerances and offers details for various repair methods depending on the extent of the damage. For DS12, the structure suffers extreme damage and the VBEs and HBEs, or the entire CoSPSW, need to be replaced.

Table 1. Test data of 19 corrugated steel plate shear wall specimens.

Specimen No.		Thickness (mm)	Aspect Ratio (L/H)	Height-to-Thickness Ratio (H/t)	Peak Inter-Story Drift (%)
Emami [9]	S-2	1.25	1.33	1184	6.10
	S-3	1.25	1.33	1184	6.10
Hos [11]	C-30	1.25	1.20	1261	6.35
	C-45	1.25	1.20	1261	6.35
	C-60	1.25	1.20	1261	6.35
Ding [12]	CSPSW-1	1.60	1.22	1687	4.00
	CSPSW-2	2.00	1.22	1687	2.20
	CSPSW-3	1.60	0.83	1687	4.00
	CSPSW-4	1.66	1.22	1687	2.10
Sudeok Shon [13]	FR-TR-V	3.20	1.69	555	8.00
	FR-TR-H	3.20	1.69	555	8.00
Cao [14]	S-1	2.93	0.96	425	2.53
	S-2	2.47	0.71	628	1.48
Zhao [15]	S-2	2.00	1.00	550	5.00
	S-3	2.00	1.00	550	4.00
	S-4	2.00	1.00	550	4.50
Wang [16]	SPSW-2	3.00	0.70	660	1.90
	SPSW-3	3.00	0.70	660	2.30
Jin [17]	CoSPSW	5.00	1.00	180	2.50

Table 2. Damage states.

Damage State	Description	Damage State	Description
1	Elastic Web Plate Buckling for Slender Corrugated Web Plate	7	HBE Local Buckling Requiring Repair
2	Initial Corrugated Web Plate Yielding	8	VBE Local Buckling Requiring Repair
3	Significant Plastic Deformation of Corrugated Web Plate	9	Corrugated Web Plate Cracking
4	Initial HBE and/or VBE Yielding	10	HBE and HBE-to-VBE Connection Cracking
5	Initial VBE Local Buckling	11	VBE Cracking
6	Initial HBE Local Buckling	12	Connection and/or Boundary Frame Failure

Table 3. Repair states and corresponding damage states.

Repair State	Description	Corresponding Damage States
1	Cosmetic repair	1,2,4,5,6
2	Replace Web Plate	3,9
3	HBE and Connection Repair	7,10
4	VBE Repair	8,11
5	Replace Boundary Elements or Frame	12

The inter-story drifts are also recorded from the test observations on the 19 specimens listed in Table 4. The median value, coefficient of variation, and the number of data points of the inter-story drift for each damage state and repair state are listed in Tables 4 and 5, respectively. Figure 2 shows the distribution of the repair states and the corresponding inter-story drift. As shown in Table 4, the median drift increases with the damage state, which indicates that the ordering of the states is proper and consistent with the damage

sequence. From Table 5 and Figure 2, it can be known that for RS1, RS2, and RS4 the results are more accurate because the number of data points is more abundant, with a smaller dispersion. For RS3, there are fewer data points and related descriptions; so, the determination of this repair state is more subjective. For RS5, as the ultimate performance of the CoSPSW is obviously affected by the wall corrugation configuration that varies with each group of test specimens, the dispersion of the data points is more obvious. Figure 2 also shows that the inter-story drift gradually increases when the repair state varies from RS1 to RS5, which further shows that the established repair state sequence is reasonable and consistent with the ideal failure sequence of the CoSPSW. It is worth noting that the height-to-thickness ratio of the specimens collected in this paper ranges from 425 to 1261, and the aspect ratio ranges from 1 to 1.33.

Table 4. The inter-story drift data of 19 tested specimens of each damage state.

DS	Median (%)	COV	Data Points
1	0.19	0.15	5
2	0.25	0.32	4
3	0.42	0.39	10
4	0.26	0.45	5
5	-	-	0
6	-	-	0
7	1.07	0.20	2
8	1.25	0.17	5
9	1.37	0.35	10
10	-	-	0
11	3.00	0.10	3
12	4.10	0.39	10

Table 5. The inter-story drift data of 19 tested specimens of each repair state.

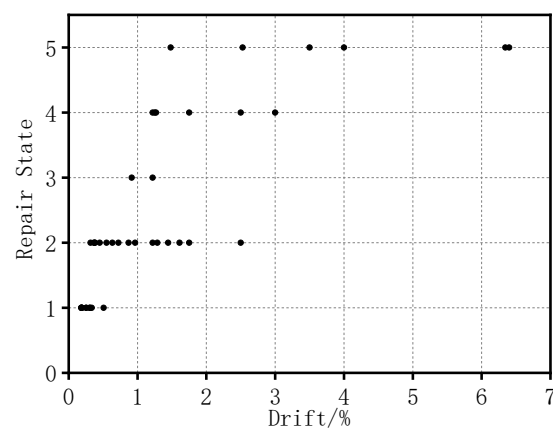| RS	Median (%)	COV	Data Points
1	0.19	0.38	14
2	0.80	0.63	20
3	1.07	0.20	2
4	1.51	0.40	8
5	4.10	0.39	10

Figure 2. Distribution diagram of repair state data and inter-story drift.

2.2. Calibration of Recommended Values of Inter-Story Drift

The damage and repair probability are estimated based on the threshold values of the structural response parameters, e.g., inter-story drift. These threshold values of different repair states are generally obtained from test observations and adjusted through the maximum likelihood method. The values of inter-story drift determined by the maximum likelihood method would be more reasonable as they can avoid the random errors caused by using the median and standard deviation of the sample data directly.

Table 6 lists the median value and standard deviation value of inter-story drift, calculated through the maximum likelihood method using Matlab. It can be seen from Table 6 that the calculated value θ_x is close to the median value of the inter-story drift in Table 5. In addition, the calculated value β_x is further adjusted for the convenience of practical application, according to the recommendation of ATC-58 [43], as in Equation (1) below. Finally, the adjusted θ_x and β values are appropriately rounded up to θ_{rec} and β_{rec} for the convenience of the design and application, as shown in Table 6.

$$\beta = \sqrt{\beta_x^2 + \beta_u^2} \tag{1}$$

where β_x is the standard deviation value calculated by the maximum likelihood method, and β_u is taken as 0.25 in order to consider uncertainty in the statistics and the limitation of the number of experimental data.

Table 6. Repair state statistics and recommended values (%).

Repair State	θ_x	β_x	β	θ_{rec}	β_{rec}
RS1	0.23	0.31	0.39	0.20	0.40
RS2	0.80	0.63	0.67	0.80	0.50
RS3	1.06	0.14	0.29	1.00	0.40
RS4	1.76	0.38	0.46	1.80	0.40
RS5	4.31	0.47	0.54	4.30	0.50

Table 7 summarizes the recommended inter-story drift θ_{rec} of each repair state and the corresponding description of the CoSPSWs and SPSWs, in which the recommended inter-story drift and repair states for the SPSWs were established by Baldvins et al. [34], based on experimental observations. As seen in Table 7, no inter-story drift was recommended for RS4 because there were not enough experimental data. The recommended inter-story drift of "Repair boundary column" for the SPSW is lower than that of the CoSPSW because the anchoring forces from the yielding of the diagonal tension field in the flat wall plates in the SPSW would increase the damage degree of the boundary column.

Table 7. Repair states and recommended inter-story drift of CoSPSWs and SPSWs.

Repair States	Recommended Inter-Story Drift		Description	
	CoSPSW	SPSW	CoSPSW	SPSW
RS1	0.002	0.004	Repair infill wall surface	
RS2	0.008	0.006	Replace infill wall	
RS3	0.01	0.015	Repair boundary beam and beam-column connection	Repair boundary column
RS4	0.018	-	Repair boundary column	Repair boundary beam and beam-column connection
RS5	0.043	0.0275	Replace boundary beam, column, or frame	

Tables 8 and 9 show the damage degrees of drift-sensitive and acceleration-sensitive nonstructural members, according to the recommendation of HAZUS-MH MR5 [41], which

are divided into four grades, namely "slight", "moderate", "severe", and "complete". The seismic performance and vulnerability assessment of the structure will be conducted in later sections using these repair states/damage states and the corresponding inter-story drift or peak floor acceleration.

Table 8. Damage states for nonstructural drift-sensitive components.

Damage States	Slight	Moderate	Extensive	Complete
Inter-story drift	0.004	0.008	0.025	0.050

Table 9. Damage states for nonstructural acceleration-sensitive components.

Damage States	Slight	Moderate	Extensive	Complete
Peak floor acceleration	0.3 g	0.6 g	1.2 g	2.4 g

3. Incremental Dynamic Analyses

3.1. Structural Models

In order to obtain the relationship between the EDP and the IM, incremental dynamic analyses were conducted on 10-story CoSPSW structures designed with PBSD [33], based on which the fragility function was developed, and the probabilistic vulnerability was assessed. For comparison, two models were studied: (i) a 10-story CoSPSW with a span of 4.5 m and a story height of 3.2 m and (ii) a 10-story SPSW using a flat steel plate with the same thickness and boundary frame as that of the 10-story CoSPSW. The floor plan is shown in Figure 3. The dead (live) load was 4.0 (2.0) kN/m^2 on the floors and 4.5 (2.0) kN/m^2 on the roof. The construction site is Class II (i.e., medium-stiff soil) within a region of Seismic Intensity 8 and Design Earthquake Group I [44]. The floor was 120 mm thick cast-in-place concrete, and the beams and columns were steel welded H-sections with rigid beam-column connections. Q235B grade steel (235 MPa design yield strength) and Q345B grade steel (345 MPa design yield strength) were used for the wall plates and frame members, respectively. The corrugation depth and wavelength of the corrugated wall plate were 100 mm and 400 mm, respectively, and the width of the subpanels was uniform. The design parameters and member sections are shown in Tables 10 and 11.
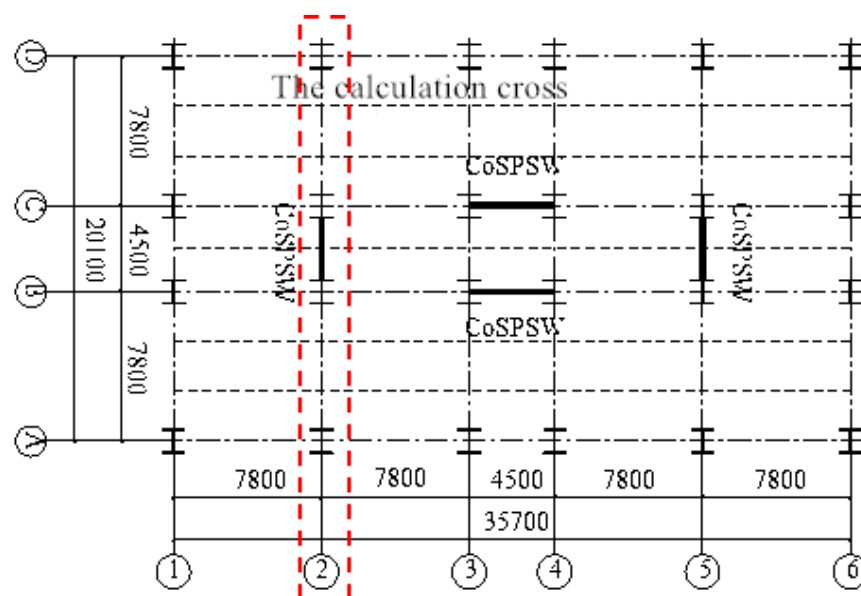

Figure 3. Floor Plan of the Structure.

Table 10. Design Parameters for the structural model.

Design Parameter	Value
Horizontal seismic influence factor	0.463
Spectral acceleration Sa/g	1.106
Fundamental period T/s	1.152
Yield drift θ_y	0.005
Target drift θ_u	0.025
Ductility coefficient μ_s	5
Ductility reduction coefficient R_μ	5
Energy correction factor γ	0.360
ξ	2.745
V_y/W	0.152

Table 11. Member Sections from of the structural model.

Floor	Columns in the Wall Plate Span *	Columns Outside the Wall Plate Span *	Wall Plate Thickness (mm)
10	H450 × 450 × 12 × 20	H350 × 350 × 16 × 18	1.8
9	H500 × 500 × 14 × 22	H400 × 400 × 16 × 18	3.0
8	H550 × 550 × 18 × 26	H400 × 400 × 16 × 20	4.0
7	H600 × 600 × 24 × 32	H450 × 450 × 16 × 22	4.9
6	H600 × 600 × 32 × 42	H450 × 450 × 20 × 26	5.6
5	H650 × 650 × 36 × 48	H500 × 500 × 20 × 26	6.3
4	H650 × 650 × 48 × 56	H500 × 500 × 24 × 28	6.9
3	H700 × 700 × 48 × 56	H550 × 550 × 24 × 28	7.3
2	H750 × 750 × 56 × 64	H550 × 550 × 28 × 32	7.6
1	H750 × 750 × 68 × 72	H600 × 600 × 28 × 36	7.8

* Note: H sections: overall depth (mm) × flange width (mm) × web thickness (mm) × flange thickness (mm).

3.2. Finite Element Models

Two 3-span structural models with wall plates in the interior span and moment frames in the exterior spans were modeled using finite element software ABAQUS (SIMULIA, 2014), as shown in Figure 4. Both the frame beams and the columns were modeled using beam element B31, while the corrugated wall plates were simplified into an equivalent braces model [45] using truss element T3D2, according to the principle of equivalent lateral stiffness and strength. The area A_{eb} and the yield strength f_{eb} of the equivalent brace model were calculated from Equation (2) and Equation (4), respectively [45]. The flat wall plates were simplified into a strip model, in which 10 equally spaced discrete tension-only strips oriented at 45° relative to the vertical were represented. The truss element T3D2 was used to model the strip, and the area of strip A_s was calculated from Equation (5). The out-of-plane displacements were restrained at all the beam-column joints, and the columns were fixed at the base. A bilinear elastoplastic constitutive model that considered the strain hardening was adopted for the steel material of the infill wall plate and the boundary members, with an elastic modulus E = 206 GPa, a strain hardening modulus E_h = 0.01E, a Poisson's ratio v = 0.3, and yield strengths of 235 MPa and 345 MPa, respectively.

$$A_{eb} = \frac{K_P l_{eb}}{2E \cos^2 \beta} \tag{2}$$

$$K_P = \frac{0.95 E q_{co} l_n t}{2 h s_{co}(1+v)} \tag{3}$$

$$f_{eb} = \frac{\tau_{cr} l_n t}{2 A_{eb} \cos \beta} \tag{4}$$

$$A_s = \frac{t_w \sqrt{L_e^2 + H_e^2}}{n_2} \cos[45° - \tan^{-1}(H_e/L_e)] \tag{5}$$

where l_{eb} is the length of the equivalent brace; q_{co} and s_{co} are the wavelength and corrugation developed length, respectively; t_w is the thickness of the wall plate; L_e and H_e are the net width and net height of the wall plate; and n_2 is the number of tension-only strips, which was taken as 10 in this study.
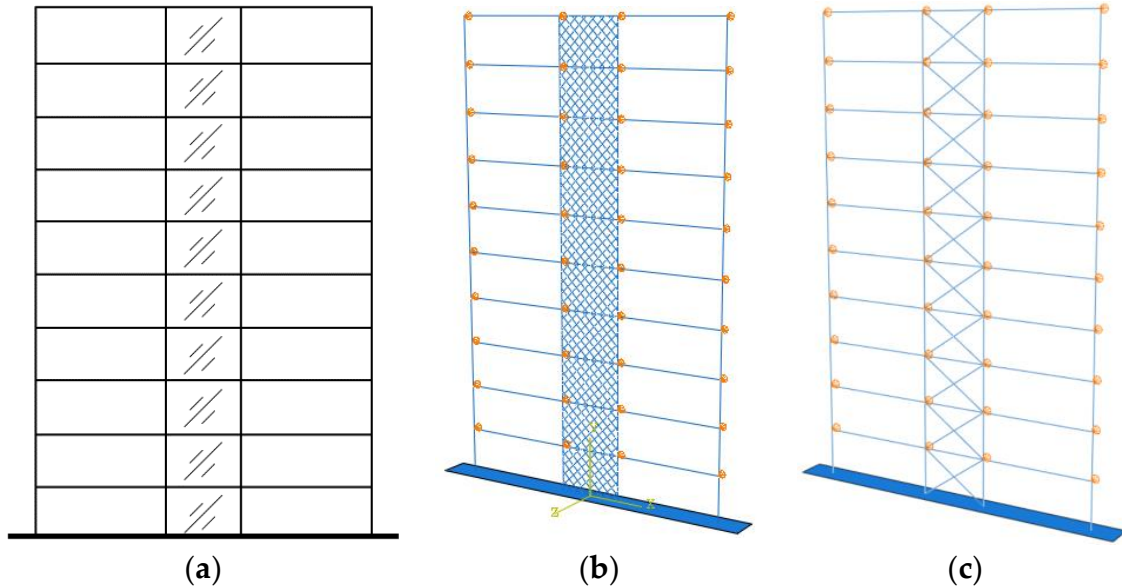

Figure 4. Finite Element Model: (**a**) the 3-span structure, (**b**) the SPSW model, and (**c**) the CoSPSW model.

The accuracy of the finite element model was validated by comparing the numerical analysis results with the experimental results. In order to accomplish the validation, the cyclic experimental specimen of a single-story CoSPSW specimen [9] and a three-story SPSW specimen [46] were considered. As shown in Figure 5, the hysteretic curve of the finite element analysis correlates well with the experiment results, which means that the equivalent braces model and the tension-only strip model are appropriate and precise in reflecting the responses of the CoSPSW and SPSW, respectively.
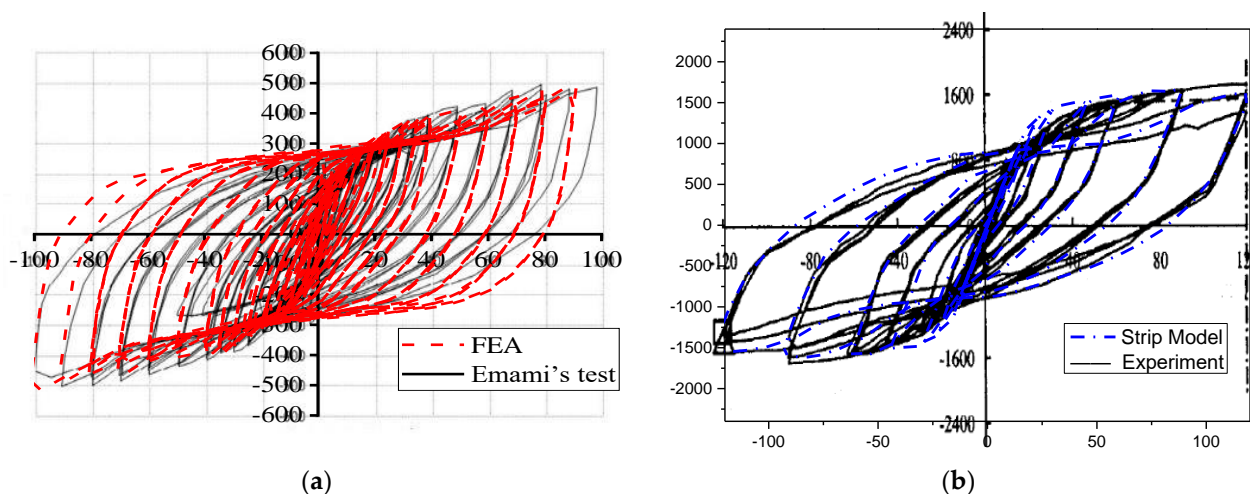

Figure 5. Validation of the finite element analysis: (**a**) validation of CoSPSW model, (**b**) validation of SPSW model.

3.3. Incremental Dynamic Analyses

Incremental dynamic analyses (IDA) were carried out on both the CoSPSW and the SPSW structures, in which additional masses were applied at the beam-column joints, and the earthquake excitation was input through the base. As shown in Table 12, ten earthquake

excitation records with a magnitude of higher than 6.5, an effective period larger than 4 s, and different spectrum characteristics were selected, according to the Chinese seismic design specification [44]. The peak ground acceleration (PGA) of the seismic excitations was adjusted from 0.1 g to 1.2 g, with an interval of 0.1 g for the incremental dynamic analyses.

Table 12. Selected Ground Motions.

Record No.	Record	Minimum Frequency (Hz)	PGA (g)	PGV * (cm/s)
RSN0169	IMPVALL.H_H-DLT352	0.09	0.35	33
RSN0174	IMPVALL.H_H-E11230	0.10	0.38	45
RSN0752	LOMAP_CAP090	0.25	0.51	38
RSN0767	LOMAP_G03090	0.13	0.56	45
RSN0953	NORTHR_MUL279	0.15	0.49	67
RSN0960	NORTHR_LOS270	0.13	0.47	41
RSN1111	KOBE_NIS090	0.13	0.48	47
RSN1485	CHICHI_TCU045N	0.05	0.51	46
RSN1602	DUZCE_BOL090	0.06	0.81	66
RSN1787	HECTOR_HEC090	0.04	0.33	45

Note: * PGV: peak ground velocity.

In this study, the inter-story drift and the peak floor acceleration were chosen as the engineering demand parameter (EDP), and the peak ground acceleration (PGA) was chosen as the intensity measure (IM), with reference to previous studies on the probabilistic assessment of various structures, including SPSWs [37]. The probabilistic seismic assessment was then employed to relate the EDPs to the IMs and derive the fragility functions. The mean and standard deviation of the EDP for a given IM were estimated by regression analysis, and the relationship between the mean EDP and IM is as follows:

$$EDP = a(IM)^b \text{ or } \ln(EDP) = b\ln(IM) + \ln(a) \qquad (6)$$

where the constants *a* and *b* are the regression coefficients obtained from the IDA analysis. It is assumed that the remaining variability in ln (EDP) for a given IM has a constant variance for all IMs, and the standard deviation can be obtained as follows [47]:

$$\zeta_{EDP|IM} = \sqrt{\frac{\sum\limits_{i=1}^{N}\left[\ln(EDP_i) - \ln\left(a(IM_i)^b\right)\right]^2}{N-2}} \qquad (7)$$

where *N* is the number of EDP-IM pairs, and EDP_i and IM_i are the values of the i-th pair.

From the incremental dynamic analyses, a large number of peak inter-story drift, peak floor acceleration, and corresponding PGA, i.e., EDP-IM, data pairs were obtained, and ln[IM = PGA] − ln[EDP = Drift] and ln[IM = PGA] − ln[EDP = PFA] are plotted in Figures 6 and 7, respectively. The values of parameters *a* and *b* can be obtained by performing regression analysis on the ln [IM = PGA] and ln [EDP = Drift] from the incremental dynamic analysis results. The coefficient R^2, which describes the quality of the fitting effect of the two parameters, was obtained through linear regression analyses, and R^2 was near 0.8 for the two EDP-IM pairs of the SPSW and CoSPSW structures, indicating a strong correlation. Therefore, the Drift-PGA and PFA-PGA data pairs were appropriate for developing the fragility functions. The lognormal distribution parameters *a* and *b*, the standard deviation $\zeta_{EDP|IM}$, and the functions were then determined and are shown in Table 13.
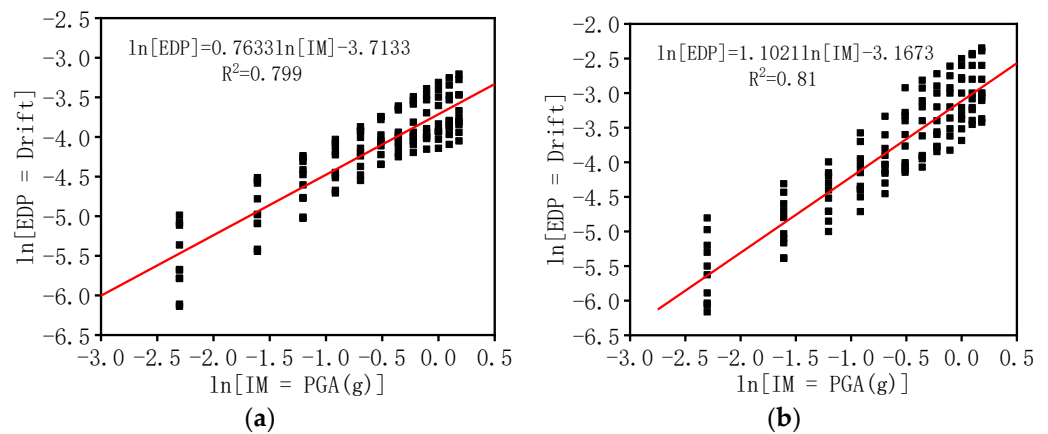
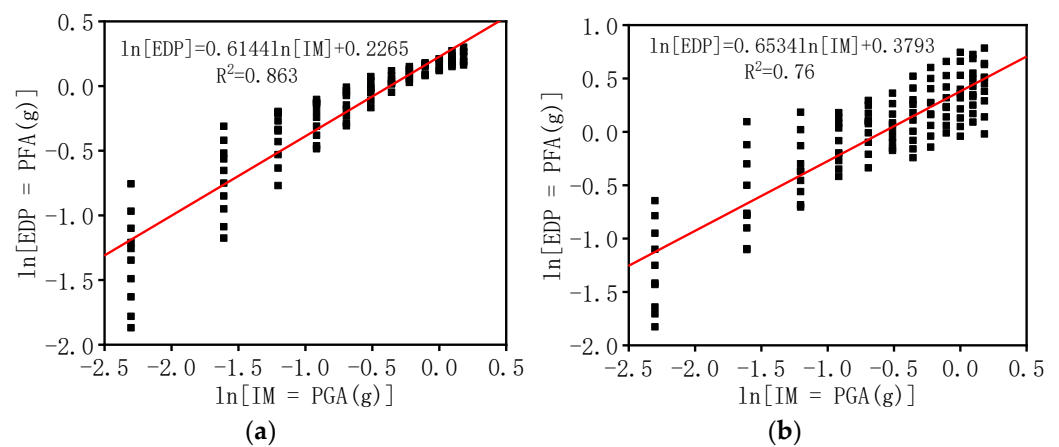**Figure 6.** Relationship between ln[IM = PGA] and ln[EDP = Drift]: (**a**) CoSPSW, (**b**) SPSW.

Figure 7. Relationship between ln[IM = PGA] and ln[EDP = PFA]: (**a**) CoSPSW, (**b**) SPSW.

Table 13. Regression coefficients, standard deviation, and function for EDP–IM data pairs.

Model	Selected		Regression Coefficients		$\zeta_{EDP|IM}$	Function
	EDP	**IM**	*a*	*b*		
CoSPSW	Drift	PGA	0.0244	0.7633	0.2792	Drift = 0.0244(PGA)$^{0.7633}$
	PFA	PGA	1.3054	0.6144	0.1882	PFA = 1.3054(PGA)$^{0.6144}$
SPSW	Drift	PGA	0.0421	1.1021	0.2919	Drift = 0.0421(PGA)$^{1.1021}$
	PFA	PGA	1.4613	0.6534	0.2810	PFA = 1.4613(PGA)$^{0.6534}$

4. Probabilistic Assessment

4.1. Fragility Functions

Assuming that the engineering demand parameter (EDP), i.e., the peak inter-story drift and the peak floor acceleration, has a lognormal distribution for a given intensity measure (IM), then the fragility function defining the probability of the EDP reaching or exceeding a certain limit state (LS) under a given IM is as follows

$$P(EDP \geq LS|IM) = 1 - \int_0^{LS} \frac{1}{\sqrt{2\pi} \cdot \zeta_{EDP|IM} \cdot EDP} \cdot e^{\left[-\frac{1}{2}\left(\frac{\ln(EDP) - \ln(a(IM)^b)}{\zeta_{EDP|IM}}\right)^2\right]} \cdot d(EDP) \tag{8}$$

Accordingly, ln (*EDP*) can be considered to have a standard normal distribution, and Equation (8) could be simplified into the following equation, using the standard normal cumulative distribution function $\Phi\,(\cdot)$:

$$P(EDP \geq LS|IM) = 1 - \Phi\left(\frac{\ln(LS) - \ln\left(a(IM)^b\right)}{\zeta_{EDP|IM}}\right) \tag{9}$$

The damage and repair probability were determined based on the threshold values of the EDP, e.g., the inter-story drift and peak-floor acceleration, which initiate different damage states and repair states. These threshold values are LS in Equations (8) and (9) and are shown in Tables 7–9. According to the considered threshold values of the repair/damage states and the regression coefficients obtained through IDA analysis, the fragility curves for the structural and nonstructural components were obtained for the 10-story CoSPSW and SPSW, respectively, and are shown in Figures 8–10.
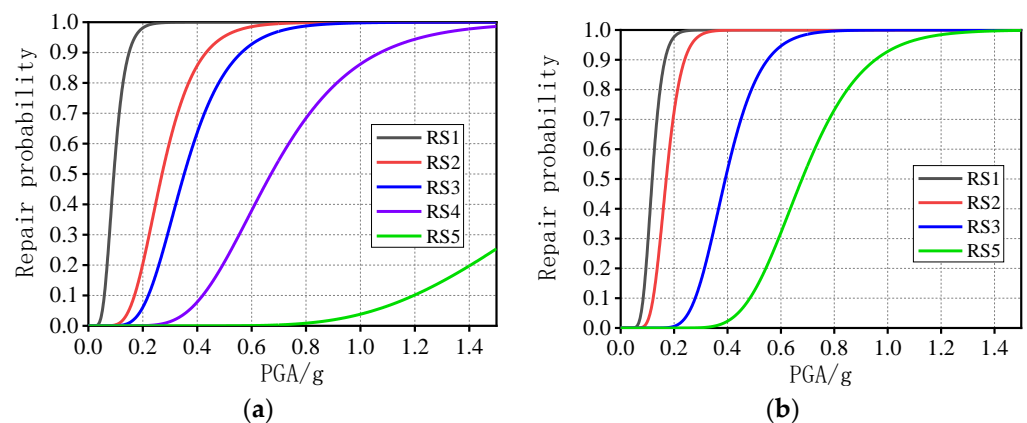

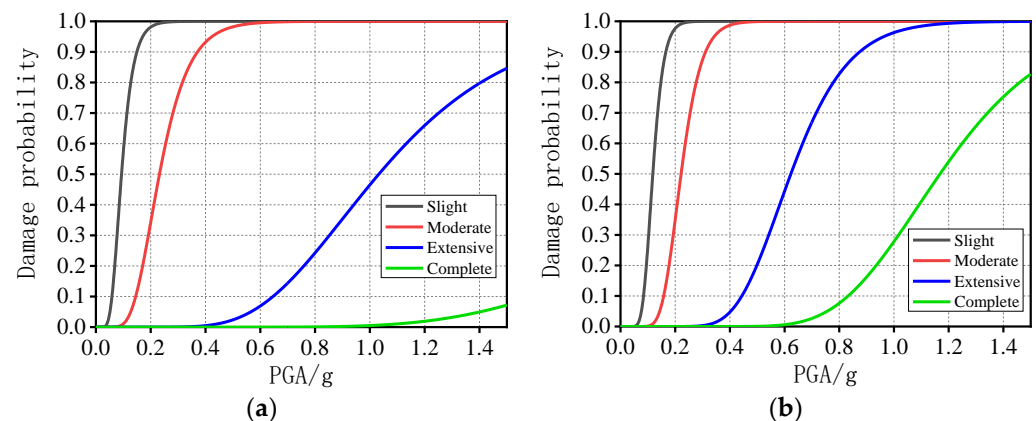**Figure 8.** Structural Fragility Curves: (**a**) CoSPSW, (**b**) SPSW.

Figure 9. Drift-sensitive nonstructural components fragility curves: (**a**) CoSPSW, (**b**) SPSW.

4.2. Seismic Vulnerability

When the variation is similar, the seismic vulnerabilities of the different structures could be compared through the 25th percentile PGA values, i.e., the PGA values corresponding to exceeding the probability of 25% [48]. The larger the 25th percentile PGA values, the better the structural performance in earthquakes, as it indicates that the structure needs to undergo higher levels of seismicity to suffer the damage level. The seismic vulnerability of the CoSPSW and the SPSW structures were then assessed by comparing the 25th percentile PGA values of the structural and nonstructural fragility curves for the damage/repair states, as shown in Figures 11–13.
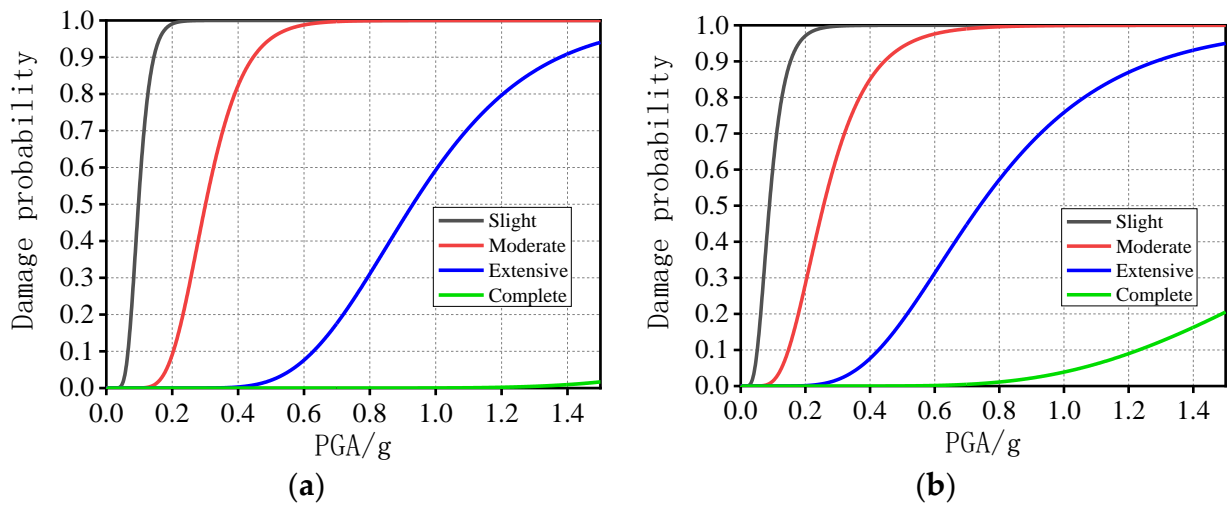
Figure 10. Acceleration-sensitive nonstructural components fragility curves: (**a**) CoSPSW, (**b**) SPSW.
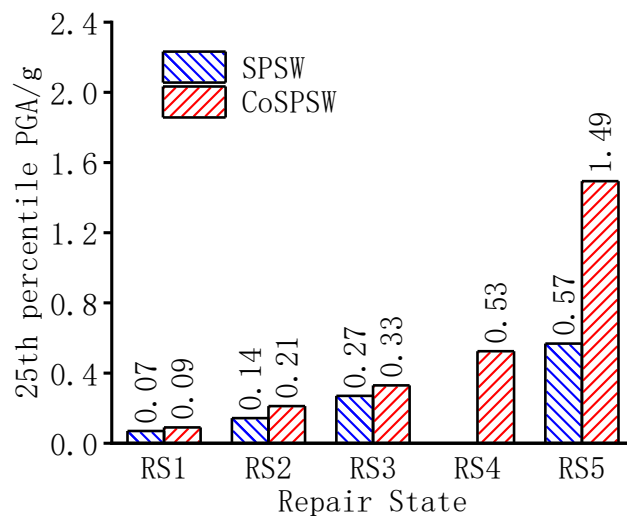

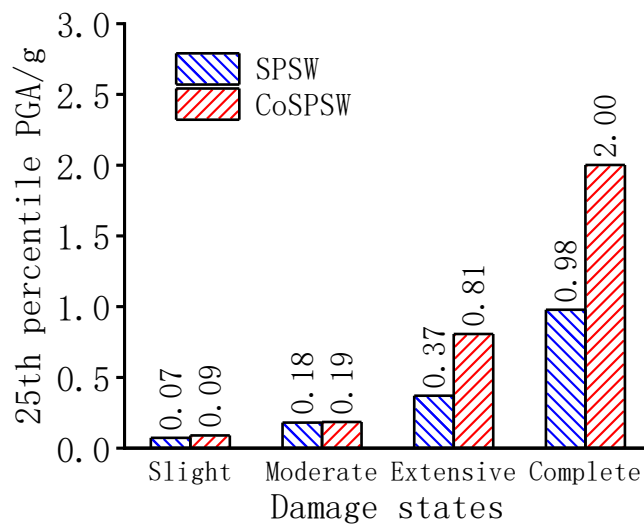**Figure 11.** The 25th percentile PGA from structural fragility curves.

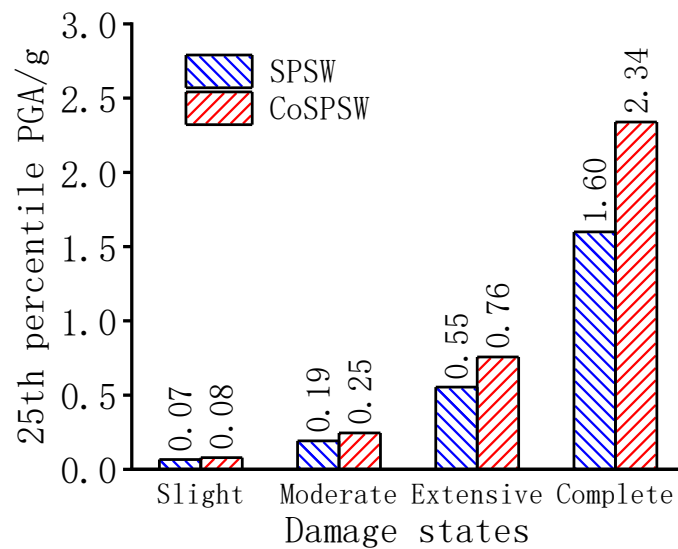**Figure 12.** The 25th percentile PGA from drift-sensitive nonstructural fragility curves.

Figure 13. The 25th percentile PGA from acceleration-sensitive nonstructural fragility curves.

It is clear from Figures 11–13 that from the RS1 to the RS5 repair states and from the "Slight" to the "Complete" damage states, the 25th percentile PGA values for both the CoSPSW structure and the SPSW structure increase significantly, indicating that the structures would experience more serious damages with the increase in seismic intensity. Furthermore, from the RS1 to the RS5 repair states, the 25th percentile PGA values of the fragility curves of the CoSPSW structure are 22%, 33%, 18%, and 62% higher than those of the SPSW structure, respectively. For the same repair method concerning the repair of the boundary column (the RS4 of the CoSPSW), the 25th percentile PGA value is 0.53 g, which is 55% higher than the RS3 of the SPSW. This indicates that for a given damage state, the CoSPSW is required to undergo higher levels of seismicity to suffer the same damage degree as the SPSW. For the drift-sensitive nonstructural damage state of "Slight" to "Complete", the 25th percentile PGA values of the fragility curves of the CoSPSW structure are 22%, 5%, 54%, and 51% higher than those of the SPSW structure, respectively. For the acceleration-sensitive nonstructural damage state of "Slight" to "Complete", the 25th percentile PGA values of the fragility curves of the CoSPSW structure are 13%, 24%, 28%, and 32% higher than those of the SPSW structure, respectively.

Therefore, as the number of damage states/repair states increases, the 25th percentile PGA values of the CoSPSW become obviously higher than those of the SPSW, which indicates that the CoSPSW has a lower seismic vulnerability and probability of structural and nonstructural damage than the SPSW structure, especially for the repair state RS5 for the structural members and the "extensive" and "complete" damage states for the non-structural members.

5. Conclusions

(1) The inter-story drift data on the seismic performance of the corrugated steel plate shear walls (CoSPSWs) were collected and analyzed. The observations on the cyclic behavior of the 19 CoSPSW test specimens have resulted in the development of twelve damage states. Five repair states were also proposed to consider the difficulty of repairing the observed damage following the earthquake, ranging from cosmetic repair to member or boundary frame replacement.

(2) In order to avoid the random error caused by the direct use of the median and standard deviation of the test data, the maximum likelihood method was used to calculate the median value and the standard deviation value of the inter-story drift. According to ATC58, the recommended median value θ_{rec} and the standard deviation value β_{rec} of the inter-story drift corresponding to the different repair states of the CoSPSW were derived and were used as the threshold value of each repair state in the fragility function.

(3) Incremental dynamic analyses (IDA) were conducted on a 10-story CoSPSW structure and a conventional steel plate shear wall (SPSW) structure with the same wall plate thickness and boundary frame. From the IDA results, the relationship between the EDP (peak inter-story drift/peak floor acceleration) and the IM (PGA) were obtained. The coefficient R^2 was approximately 0.8, which meant that the data-fitting was relatively precise. Based on the relationship between the EDP and the IM, the regression coefficients in the fragility function were obtained.

(4) According to the recommended threshold values of the repair/damage states and the regression coefficients obtained through incremental dynamic analyses (IDA), fragility curves were obtained for the 10-story CoSPSW structure and the SPSW structure, respectively. It was shown that the 25th percentile PGA of the CoSPSW was higher than that of the SPSW for various repair states and damage states, especially for the repair state RS5 for the structural members and the "extensive" and "complete" damage states for the non-structural members. Therefore, the CoSPSW structure had a lower damage degree and better seismic behavior than the SPSW structure.

Author Contributions: Q.Z. provided the idea and gave professional seismic guidance on the corrugated steel plate shear wall; Z.T. analyzed the engineering data and wrote the paper draft; Y.Z. conducted the finite element analyses and prepared the paper draft; C.Y. conducted the validation of the finite element model and provided supervision of the writing process. All authors have read and agreed to the published version of the manuscript.

Institutional Review Board Statement: Not applicable.

Informed Consent Statement: Not applicable.

Data Availability Statement: Not applicable.

Conflicts of Interest: The authors declare no conflict of interest.

References

1. Montgomery, C.J.; Medhekar, M.; Lubell, A.S. Unstiffened Steel Plate Shear Wall Performance under Cyclic Loading. *J. Struct. Eng.* **2001**, *127*, 973–975. [CrossRef]
2. Berman, J.W.; Bruneau, M. Plastic Analysis and Design of Steel Plate Shear Walls. *J. Struct. Eng.* **2003**, *129*, 1448–1456. [CrossRef]
3. Berman, J.W. Seismic behavior of code designed steel plate shear walls. *Eng. Struct.* **2011**, *33*, 230–244. [CrossRef]
4. Driver, R.G. Cyclic Test of Four-Story Steel Plate Shear Wall. *J. Struct. Eng.* **1998**, *124*, 112–120. [CrossRef]
5. Berman, J.W.; Bruneau, M. Capacity Design of Vertical Boundary Elements in Steel Plate Shear Walls. *Eng. J. Am. Inst. Steel Constr. Inc.* **2008**, *45*, 57–71.
6. *JGJ/T 380-2015*; Technical Specifications for Steel Plate Shear Walls. China Construction Industry Press: Beijing, China, 2016. (In Chinese)
7. Berman, J.W.; Celik, O.C.; Bruneau, M. Comparing hysteretic behavior of light-gauge steel plate shear walls and braced frames. *Eng. Struct.* **2005**, *27*, 475–485. [CrossRef]
8. Berman, J.W.; Bruneau, M. Experimental investigation of light-gauge steel plate shear walls. *J. Struct. Eng.* **2005**, *131*, 259–267. [CrossRef]
9. Emami, F.; Mofid, M.; Vafai, A. Experimental study on cyclic behavior of trapezoidally corrugated steel shear walls. *Eng. Struct.* **2013**, *48*, 750–762. [CrossRef]
10. Stojadinovic, B.; Tipping, S. Structural testing of corrugated sheet steel shear walls. In Proceedings of the19th International Specialty Conferences on Cold-Formed Steel Structures, Rolla, MO, USA, 14–15 October 2008.
11. Hosseinzadeh, L.; Emami, F.; Mofid, M. Experimental investigation on the behavior of corrugated steel shear wall subjected to the different angle of trapezoidal plate. *Struct. Des. Tall Spec. Build.* **2017**, *2*, e1390. [CrossRef]
12. Ding, Y.; Deng, E.F.; Zong, L.; Dai, X.; Lou, N. Cyclic tests on corrugated steel plate shear walls with openings in modularized-constructions. *J. Constr. Steel Res.* **2017**, *138*, 675–691. [CrossRef]
13. Sudeok, S.; Mina, Y.; Seungjae, L. An Experimental Study on the Shear Hysteresis and Energy Dissipation of the Steel Frame with a Trapezoidal-Corrugated Steel Plate. *Materials* **2017**, *10*, 261. [CrossRef]
14. Cao, Q.; Huang, J. Experimental study and numerical simulation of corrugated steel plate shear walls subjected to cyclic loads. *Thin-Walled Struct.* **2018**, *127*, 306–317. [CrossRef]

15. Qiu, J.; Zhao, Q.H.; Yu, C.; Li, Z.X. Experimental studies on cyclic behavior of corrugated steel plate shear walls. *J. Struct. Eng.* **2018**, *144*, 4018200. [CrossRef]

16. Wang, W.; Ren, Y.; Lu, Z. Experimental study of the hysteretic behaviour of corrugated steel plate shear walls and steel plate reinforced concrete composite shear walls. *J. Constr. Steel Res.* **2019**, *160*, 136–152. [CrossRef]

17. Jin, S.S.; Wang, Q.Y.; Zhou, J.; Bai, J.L. Numerical and experimental investigation of assembled multi-grid corrugated steel plate shear walls. *Eng. Struct.* **2022**, *251*, 113544. [CrossRef]

18. Emami, F.; Mofid, M. On the hysteretic behavior of trapezoidally corrugated steel shear walls. *Struct. Des. Tall Spec. Build.* **2014**, *23*, 94–104. [CrossRef]

19. Edalati, S.A.; Yadollahi, Y.; Pakar, I.; Emadi, A.; Bayat, M. Numerical study on the performance of corrugated steel shear walls. *Wind Struct.* **2014**, *19*, 405–420. [CrossRef]

20. Kalali, H.; Hajsadeghi, M. Hysteretic performance of SPSWs with trapezoidally horizontal corrugated web-plates. *Steel Compos. Struct.* **2015**, *19*, 277–292. [CrossRef]

21. Zhao, Q.H.; Sun, J.H.; Li, Y.; Li, Z.X. Cyclic analyses of corrugated steel plate shear walls. *Struct. Des. Tall Spec. Build.* **2017**, *26*, e1351. [CrossRef]

22. Dou, C.; Jiang, Z.Q.; Pi, Y.L.; Guo, Y.L. Elastic shear buckling of sinusoidally corrugated steel plate shear wall. *Eng. Struct.* **2016**, *121*, 136–146. [CrossRef]

23. Farzampour, A.; Mansouri, I.; Hu, J.W. Seismic behavior investigation of the corrugated steel shear walls considering variations of corrugation geometrical characteristics. *Int. J. Steel Struct.* **2018**, *18*, 1297–1305. [CrossRef]

24. Bahrebar, M.; Kabir, M.; Zirakian, M.; Hajsadeghi, M.; Lim, J. Structural performance assessment of trapezoidally-corrugated and centrally-perforated steel plate shear walls. *J. Constr. Steel Res.* **2016**, *122*, 584–594. [CrossRef]

25. Bahrebar, M.; Lim, J.; Clifton, G.; Zirakian, T.; Shahmohammadi, A.; Hajsadeghi, M. Perforated steel plate shear walls with curved corrugated webs under cyclic loading. *Structures* **2020**, *24*, 600–609. [CrossRef]

26. Farzampour, A.; Yekrangnia, M. On the behavior of corrugated steel shear walls with and without openings. In Proceedings of the Second European Conference on Earthquake Engineering and Seismology, Istanbul, Turkey, 25–29 August 2014.

27. Farzampour, A.; Laman, J.A. Behavior prediction of corrugated steel plate shear walls with openings. *J. Constr. Steel Res.* **2015**, *114*, 258–268. [CrossRef]

28. Farzampour, A.; Mansouri, I.; Lee, C.H.; Sim, H.B.; Hi, J.W. Analysis and design recommendations for corrugated steel plate shear walls with a reduced beam section. *Thin-Walled Struct.* **2018**, *132*, 658–666. [CrossRef]

29. Masoud, H.A.; Mahna, S. Seismic behavior of steel plate shear wall with reduced boundary beam section. *Thin-Walled Struct.* **2018**, *116*, 169–179. [CrossRef]

30. Fang, J.; Bao, W.; Ren, F.; Guan, T.; Xue, G.; Jiang, J. Experimental study of hysteretic behavior of semi-rigid frame with a corrugated plate. *J. Constr. Steel Res.* **2020**, *174*, 106–119. [CrossRef]

31. Shariati, M.; Faegh, S.S.; Mehrabi, P.; Bahavarnia, S.; Zandi, Y.; Masoom, D. Numerical study on the structural performance of corrugated low yield point steel plate shear walls with circular openings. *Steel Compos. Struct.* **2019**, *33*, 569–581. [CrossRef]

32. Yu, Y.J.; Chen, Z.H. Rigidity of corrugated plate sidewalls and its effect on the modular structural design. *Eng. Struct.* **2018**, *175*, 191–200. [CrossRef]

33. Zhao, Y. Lateral Behavior and Design Method of Corrugated Steel Plate Shear Walls. Master Thesis, Tianjin University, Tianjin, China, 2018. (In Chinese).

34. Baldvins, N.M.; Berman, J.W.; Lowes, L.N.; Janes, T.M. Fragility functions for steel plate shear walls. *Earth. Spectra.* **2012**, *28*, 405–426. [CrossRef]

35. Negar, M.; Epackachi, S. Fragility functions for steel-plate concrete composite shear walls. *J. Constr. Steel Res.* **2019**, *167*, 105776. [CrossRef]

36. Wang, M.; Guo, Y.; Yang, L. Damage indices and fragility assessment of coupled low-yield-point steel plate shear walls. *J. Build. Eng.* **2021**, *11*, 103010. [CrossRef]

37. Zhang, J.; Zirakian, T. Probabilistic assessment of structures with SPSW systems and LYP steel infill plates using fragility function method. *Eng. Struct.* **2015**, *85*, 195–205. [CrossRef]

38. Jiang, L.; Hong, Z.; Hu, Y. Effects of various uncertainties on seismic risk of steel frame equipped with steel panel wall. *Bul. Earth. Eng.* **2018**, *16*, 5995–6012. [CrossRef]

39. Hu, Y.; Zhao, J.H. Seismic risk assessment of steel frames equipped with steel panel wall. *Struct. Des. Tall Spec. Build.* **2017**, *26*, e1368. [CrossRef]

40. Bu, H.; He, L.; Jiang, H. Seismic fragility assessment of steel frame structures equipped with steel slit shear walls. *Eng. Struct.* **2021**, *249*, 113328. [CrossRef]

41. *HAZUS-MH MR5*; Earthquake Loss Estimation Methodology—Technical and User's Manual. Department of Homeland Security, Federal Emergency Management Agency, Mitigation Division: Washington, DC, USA, 2010.

42. *FEMA 352*; Recommended Post-Earthquake Evaluation and Repair Criteria for Welded Steel Moment-Frame Buildings. Safety Council for the Federal Emergency Management Agency: Washington, DC, USA, 2000.

43. *ATC-58*; Guidelines for Seismic Performance Assessment of Buildings. Safety Council for the Federal Emergency Management Agency, Applied Technology Council: Redwood, CA, USA, 2009.

44. *GB50011-2010*; Code for Seismic Design of Buildings. China Architecture and Building Press: Beijing, China, 2010. (In Chinese)

45. Jiang, W.W.; Jin, H.J.; Sun, F.F. Research on simplified analysis models of non-buckling corrugated steel shear walls. *Pro. Steel Build. Struct.* **2019**, *21*, 61–71. (In Chinese)

46. Park, H.G.; Kwack, J.H.; Jeon, S.W.; Kim, W.K.; Choi, I.R. Framed steel plate wall behavior under cyclic lateral loading. *J. Struct. Eng.* **2007**, *133*, 378–388. [CrossRef]

47. Baker, J.W.; Cornell, C.A. Vector-valued ground motion intensity measures for probabilistic seismic demand analysis. In *PEER Report*; College of Engineering, University of California: Berkeley, CA, USA, 2006.

48. Zhang, J.; Huo, Y.; Brandenberg, S.J.; Kashighandi, P. Effects of structural characterizations on fragility functions of bridges subject to seismic shaking and lateral spreading. *Earth. Eng. Eng. Vibr.* **2008**, *7*, 369–382. [CrossRef]